

Reverberation lags viewed in hard X-rays from an accreting stellar-mass black hole

Bei You^{1*}, Wei Yu^{2,3*}, Adam Ingram⁴, Barbara De Marco⁵,
 Jin-Lu Qu², Zong-Hong Zhu^{6,1}, Andrea Santangelo³, Sai-En Xu¹

¹Department of Astronomy, School of Physics and Technology, Wuhan University, Wuhan, 430072, China.

²Key Laboratory of Particle Astrophysics, Institute of High Energy Physics, Chinese Academy of Sciences, Beijing, 100049, China.

³Institut für Astronomie und Astrophysik, Kepler Center for Astro and Particle Physics, Eberhard Karls Universität, Sand 1, 72076, Tübingen, Germany.

⁴School of Mathematics, Statistics, and Physics, Newcastle University, Newcastle upon Tyne, NE1 7RU, United Kingdom.

⁵Departament de Física, EEBE, Universitat Politècnica de Catalunya, Av. Eduard Maristany 16, 08019, Barcelona, Spain.

⁶Department of Astronomy, Beijing Normal University, Beijing, 100875, China.

*Corresponding author(s). E-mail(s): youbei@whu.edu.cn; yuwei@ihep.ac.cn;

Abstract

Accreting black holes are thought to swallow matter in the form of a disk and a hot cloud of plasma that glows brightly in X-rays, known as the corona. The X-ray emitting region is far too small to be directly imaged, but rapid variability of the X-ray signal can be used to infer the geometry by measuring time lags caused by material propagating towards the black hole and by coronal X-rays reflecting off the disk to imprint a reverberation lag. Reverberation lags can be recognized by characteristic spectral features, including an iron emission line at ~ 6.4 keV and a broad Compton hump peaking at ~ 30 keV. These reverberation features have both previously been detected for a few supermassive black holes in active galactic nuclei (AGNs). However, it is much more challenging to detect reverberation lags from stellar-mass black holes because they are more than a million times smaller. Previous reverberation lag measurements for stellar-mass black holes in X-ray binary systems have thus been limited to energies below 10 keV. Here we report on the first detection of the Compton hump reverberation feature from an X-ray binary, achieved by measuring lags in

the broad energy range of $\sim 1 - 150$ keV. The accompanying detection of an iron line feature confirms the scenario of X-ray reverberation and provides strong evidence that the accretion flows in AGNs and X-ray binaries are governed by an ubiquitous process. Reverberation lags are prominent only in the most rapid variability, whereas lags in the slower variability are commonly attributed to propagating mass accretion rate perturbations. Our lag measurements up to the highest energy to date reveal that this lag in the slower variability evolves dramatically on timescales of days.

A black hole X-ray binary (BHXR) emission from the central region around the BH when it is triggered into an outburst[1]. The low energy (soft) photons (below a few keV) from the outer disk are inverse Compton scattered within the inner hot flow and/or jet near the BH, accounting for the observed high energy (hard) power-law emission, up to a cutoff energy of $\simeq 100$ keV. In this work, we refer to the X-ray Compton scattering source as the corona. During a typical outburst, an X-ray binary transitions from the corona-dominated *hard state* to the disk-dominated *soft state* and back again, before fading once more into quiescence. The X-ray emission is highly variable on time-scales of milliseconds to tens of seconds [2], so X-ray timing analysis is a very powerful tool for probing the innermost flow around accreting BHs [3–9]. When long timescales of seconds to tens of seconds are isolated by Fourier analysis (i.e., considering Fourier frequencies lower than 1 Hz), variations in higher energy (harder) X-rays are seen to lag behind variations in lower energy (softer) X-rays. This is the so-called ‘hard lag’. Such a low-frequency hard lag is thought to originate from fluctuations in the mass accretion rate, which propagate from the outer disk to the central corona [10, 11]. If the corona is large, a significant hard lag will also be contributed by the extra light travel time associated with higher energy photons that have experienced more Compton scattering events [12]. The propagation of fluctuations in the disk arises due to turbulence induced by the magneto-rotational instability [13]. However, our understanding of this process has historically been limited by past measurements of the hard lag usually only being available in the < 30 keV energy range, whereas the corona radiates strongly up to energies > 100 keV. [10, 14–17].

The Comptonized photons out of the corona can partially scatter back to the outer cold disk, where they are reprocessed, producing the observed reflection features from 0.5 keV to hundreds of keV [18–20], which include the relativistic iron K emission line at $E \sim 6.4$ keV and the Compton hump at $E \sim 20$ -70 keV [21, 22]. This disk reflection component is expected to lag behind the emission from a variable corona due to light-crossing delays, producing X-ray reverberation features [6, 23].

Whereas hard lags dominate at low Fourier frequencies, reverberation lags can be seen at high Fourier frequencies, i.e., in the fastest variability. The iron K reverberation lag and the Compton hump lag were first discovered in active galactic nuclei (AGNs) [24, 25]. The Fourier frequency of $\sim 10^{-4}$ Hz at which these lags were discovered corresponds to $\sim 10^2$ Hz for an X-ray binary, since all variability timescales are thought to scale linearly with BH mass [26, 27]. Searching for high-frequency lags in BHXRBS has, therefore, recently been a major focus in X-ray timing studies [2, 4]. However, mass scaling makes detection challenging, since the ~ 1 ks lag observed for AGNs with a $\sim 10^7 M_\odot$ BH corresponds to only ~ 1 ms for an X-ray binary with a $10 M_\odot$. Nonetheless, iron K reverberation lags have been observed

[16, 17, 28] using high throughput soft X-ray detectors, but the Compton hump lag has not been found yet despite extensive searches.

The frontier for X-ray timing is thus to extend the analysis to higher energy bands, which is vital for gaining a complete understanding of the accretion flow close to the BHs and the associated physical processes. This is now possible with the Hard X-ray Modulation Telescope (*Insight*-HXMT) [29]. As one of the three instruments in *Insight*-HXMT, the high energy X-ray Telescope (HE) can detect X-ray photons in the 20–250 keV energy range. The effective area at $E = 20 - 100$ keV is about 0.5 m^2 , and decreases to $\sim 0.1 \text{ m}^2$ at $E = 200$ keV. In the past four years, *Insight*-HXMT has made significant contributions to the spectral and timing analysis of BHXRBS. In the latest BHXR catalog of *Insight*-HXMT, MAXI J1820+070 is one of the brightest sources, which makes it the most promising candidate to probe the timing and spectral aspects of BHXR in the high energy band, ensuring high X-ray counts and excellent statistics [22, 30]. In this work, we focus on the timing analysis of high energy radiation from the corona, and mainly concentrate on the *Insight*-HXMT observations that catch the source in the rising hard state (MJD = 58192–58286). Fig. 1A shows the *Insight*-HXMT light curves from the low-energy (LE, from 1 to 10 keV), medium-energy (ME, from 10 to 30 keV), and high-energy (HE, from 27 to 150 keV) instruments (see ‘Methods’ for a description of the data reduction). The hardness-intensity (HID) diagram, defined as the total 1–10 keV count rate (in units of counts per second) versus the ratio of hard (3–10 keV) to soft (1–3 keV) count rates, is plotted in Fig. 1B. Owing to the enormous size of the dataset, we describe only the timing results of six epochs of the total *Insight*-HXMT observations (see Table 1). These epochs were selected for their lengthy observations, each capturing a different characteristic phase of the hard state. The first three epochs cover the period between the first observation and the light curve peak, and the remaining three epochs cover the period of the light curve decay. These six epochs of interest are colored in Fig. 1, corresponding to MJD = 58192, 58194, 58200, 58217, 58245, and 58286.

Frequency-dependent time lags

The spectral fits to the *Insight*-HXMT spectra of MAXI J1820+070 show that the disk reflection flux is comparable with the corona Comptonization flux below 70 keV at early epochs of the rising hard state (see Supplementary Fig. 1 in [22]). In contrast, the emission at 70–150 keV is dominated by the cutoff power law of the corona Comptonization, which thus can be taken as a good reference to study the X-ray reverberation mapping between the corona and disk. We perform frequency-resolved timing analysis for the six epochs and measure the frequency-dependent time lag between the 70–150 keV and the 27–70 keV emission, as well as between the 70–150 keV and the 4–10 keV emission. Fig. 2 shows the frequency-dependent time lags for the first two epochs of *Insight*-HXMT (P0114661001 and P0114661002). In the first epoch (left panel), the 70–150 keV emission lags behind the two softer bands (4–10 keV and 27–70 keV) at low frequencies of < 1 Hz (hard lag), while it leads both softer bands at high frequencies (soft lag).

Such high-frequency soft lags detected in the response of both the 27–70 keV and the 4–10 keV emission to the variable hard (70–150 keV) X-ray flux could be attributed to a delayed response (reverberation) of the disc component to variations of the corona, given the presence of the Compton hump and the iron K line significantly contributing to the flux in each of the

two bands. This will be further justified below by studying the energy-dependent lag at the frequency range where these soft lags are detected.

We also note that, at the highest frequencies, the lag crosses zero and becomes hard once more. This is consistent with the expectations of phase-wrapping, whereby the measured lag changes sign when the true (intrinsic) time delay, τ_{int} , exceeds the variability timescale associated with the Fourier frequency (analogous to car wheels appearing to run backwards in a film due to the rotation rate of the wheels being greater than the frame rate of the camera). We find that this characteristic phase-wrapping frequency is approximately an order of magnitude higher for the iron K reverberation than for the Compton hump reverberation. Similar differences in reverberation frequencies between the Fe-K and Compton hump bands have not been reported in AGNs.

In the simplest case, the characteristic phase-wrapping frequency f_{wrap} is related to the intrinsic delay via $f_{\text{wrap}} = 1/(2\tau_{\text{int}})$. Adopting a black hole mass of $10M_{\odot}$, and using the observed phase-wrapping frequencies in epoch 1, we estimate that the iron line reverberation originates from $R_{\text{Fe}} \approx 51r_g$ and the Compton hump from $R_{\text{CH}} \approx 145r_g$ (where $r_g = GM/c^2$). These distances should be interpreted as weighted means over all possible light-travel paths of the Comptonised photons to the disc, and can be significantly larger than the minimum light-travel distance set by the X-ray source height and the inner disc radius [31–33].

These estimates are broadly consistent with the scenario in which the ionization state of the accretion disc depends on radius: closer to the black hole, the disc is more heavily irradiated and therefore more highly ionized, enhancing the iron line strength, whereas the strength of the Compton hump is largely independent of ionization state [19]. This implies that the iron line emission originates from a more compact region than the Compton hump, naturally producing a higher characteristic phase-wrapping frequency. More discussion on the difference in detection frequency of the soft lag between the 27–70 keV and the 4–10 keV emission is provided in the Supplementary Text.

In the second epoch, just two days after the first epoch, the high-frequency soft lags of both the 27–70 keV and the 4–10 keV emission are highly suppressed (see the right panel of Fig. 2), while the low-frequency hard lags show a substantial increase. This combination suggests that there must have been a dramatic evolution of the accretion flow on a daily timescale. To investigate the origin of this lag evolution, we further examine the energy-dependent lags below.

High-frequency lag spectrum

As shown in Fig. 2, the observation at the first epoch is the only one in which the soft lags between 70–150 keV and 27–70 keV are detected. The soft lags fall within the frequency range of approximately 2–60 Hz. We, therefore, estimate energy-dependent lags in this frequency range for the first epoch by measuring the lag between several narrow ‘subject bands’ and one common ‘reference band’. We choose 1–10 keV as the reference band, except we remove photons from the current subject band to prevent noise correlation. The resulting lag-energy spectrum is plotted in Fig. 3 (red shaded region). In the energy band below 10 keV, the lag spectrum displays a broad feature that aligns with the characteristics of a relativistically broadened iron line. Above 10 keV, the lag rises to a maximum at ~ 30 keV and decreases at higher energies. Therefore, the overall lag spectrum in the 10–100 keV range resembles the

Compton hump in the energy spectrum of the disk reflection. This is the first detection of a Compton hump feature in the lag spectrum of a stellar-mass black hole X-ray binary. The presence of features that resemble the iron K and the Compton hump in the lag spectrum confirm the X-ray reverberation to be the physical origin of the observed high-frequency soft lag [24, 25].

It is generally thought that AGNs are mass-scaled-up XRBs [26, 27]. The iron K and Compton hump reverberation lags have also been detected in three AGNs to date, i.e., MCG-5-23-16, SWIFT J2127.4+5654 and NGC 1365 [24, 25]. We plot the lag spectra of these three AGNs in Fig. 3 to compare it with the reverberation lags of the XRB. The AGN lag-energy spectra are directly taken from Zoghbi et al. [24] and Kara et al. [25] without any modification of the original data. Despite their diverse shapes, the AGN lag spectra show substantial overlap with the XRB lag spectrum, particularly in the case of MCG-5-23-16, consistent with the expected linear scaling of the reverberation lag amplitude with black hole mass ($\tau \propto M_{\text{BH}}$). Notably, the masses of these three AGNs are all on the order of $10^7 M_{\odot}$ [34–38], differing by six orders of magnitude from MAXI J1820+070, well matching the observed differences in lag magnitude. This provides the strongest evidence of the mass scaling of reverberation lag amplitude between stellar-mass black holes and AGNs, offering observational support for a ubiquitous process in the accretion flows surrounding both stellar-mass and supermassive black holes.

Evolution of high-frequency lag spectrum

The timing analysis of *NICER* data showed the presence of soft lags in low energy bands (2-5 keV vs. 0.5-1 keV), likely arising from X-ray reverberation, which could be detected throughout all the epochs of the outburst of the source before it transitioned to the soft state [33]. However, by extending the time lag analysis to much higher energy bands, i.e., the 70-150 keV v.s. 27-70 keV, we find that the reverberation lags are highly suppressed after the first epoch (see the right panel of Fig. 2).

To further investigate the physical origin of high-energy soft lags and their evolution, as illustrated in Fig. 2, we then focus on analyzing the observations by the HE instrument. The frequency range of the soft lag, estimated using the lag-frequency spectra from quasi-simultaneous *NICER* data (within ± 1 day), is employed to derive the lag-energy spectra for the hard X-rays and to analyze their evolution during the rising hard state. Fig. 4 presents the lag-energy spectra at six epochs between MJD 58192 and 58286. The lag is measured between each small energy bin and a broad reference band (27-150 keV), with the bin of interest removed to avoid noise correlation. The panel (a,b) corresponds to the first and second epoch (MJD = 58192 and 58194, respectively) in the rising branch of the HID, and the panel (c-e) corresponds to the flat branch of the HID, and the panel (f) corresponds to the decaying branch of the HID. It is evident that at the onset of the outburst, high-energy photons reach the observer first, followed by lower-energy reflected photons, leading to a decrease in lag with increasing energy, ranging from approximately +0.4 ms to -0.5 ms (panel a). As the flux from the source increases rapidly (see panel b for epoch 2), the lag-energy spectra exhibit significant changes, pivoting around 60 keV so that high-energy photons from the Comptonization tail ($E > 70$ keV) arrive later than the low-energy photons arising from reflection.

As the source flux reaches its peak during the rising hard state (e.g., epoch 3), the spectrum becomes predominantly governed by hard lags, which linearly increase with energy (in logarithm) between 30-150 keV, ranging from ~ -1 ms to $\sim +7$ ms. It can be seen that the high-energy photons lag the low-energy photons by almost ~ 8 ms at this peak flux. During the flux-decreasing phase after leaving the peak, the lags start to decrease. Compared with the initial phase (panel a), where the low-energy photons lag the high-energy photons by < 1 ms, it becomes evident that the lag behavior evolves significantly throughout the hard state. We also find that at the end of the hard state, when the X-ray count rate is quite low, the lags weakly depend on the photon energy, and their amplitude is highly reduced, similar to early *Insight-HXMT* observations during the outburst.

From the high-frequency lag–energy spectra, it is apparent that with the increase in source brightness, the soft lags associated with reverberation are rapidly obscured by the strengthening hard lags. Such hard lags have been extensively observed and studied in BHXRBS, and are widely believed to result from inward-propagating perturbations in the mass accretion rate [10, 11, 39], which typically decrease with increasing Fourier frequency. Previous studies have shown that the decreasing trend of time lags with frequency can be effectively described by a power-law model [40, 41]. Due to the frequency-dependent decay of hard lags, they typically have little impact on the high-frequency part of the lag spectrum, but this holds only when their amplitude is relatively small. To further investigate the impact of such hard lags on the high-frequency lag spectrum, we next turn to an analysis of the low-frequency lag–energy spectra, which are usually dominated by propagation-induced hard lags.

Low-frequency lag spectrum and its evolution

We measured the inter-band time delays by averaging over the frequencies (0.1-1 Hz) where the hard lag is predominant, as shown in Fig. 2. The lag is measured between each energy bin and a broad reference band (1-10 keV). The derived lag spectrum and its evolution for different epochs are plotted in Fig. 5. Lag–energy spectra were also reported by Wang et al. [42] in the 1–10 Hz range, but our choice of the 0.1–1 Hz band better isolates the dominant hard lag component and, in addition, includes the earliest stages of the outburst that were not covered in their study.

At epoch 1, the time-lag shows only a weak dependence on photon energy. By epoch 2, however, the low-frequency hard lags increase rapidly—by a factor of about five—and become more pronounced toward the high-energy end (Fig. 5). As the amplitude grows, the hard lags begin to extend into higher frequencies and gradually suppress the soft lags (Fig. 4; see also Fig. 2), providing a plausible explanation for the disappearance of high-energy reverberation lags after epoch 1.

After epoch 3, i.e., the peak of the count rate, the time-lag spectra soften with a drop of the lag in the high-energy end. The magnitude of the hard lag shows a positive correlation with the count rate (see Extended Data Fig. 3). Notably, the evolution of hard lags is primarily pronounced at higher energies and becomes increasingly significant as the energy rises. No obvious evolution of hard lags is observed below 30 keV.

The hard lags are thought to be predominantly due to perturbations of the mass accretion rate propagating inward within the hot corona [10, 11, 39]. The propagation of the fluctuations leads to the different perturbations of the mass accretion rate at various radii, i.e.,

$\dot{m}(r,t)$, which modulates the X-ray emission from the corona. In order to calculate the time-lags between the low energy (soft) (E_s) and high energy (hard) bands (E_h), a simple law of radial emissivity profile in these bands is usually assumed, e.g., $\propto r^{-\gamma}$. With this prescription, propagating mass accretion rate fluctuations can be converted into energy-dependent flux variations, as $L(E,t) \propto \dot{m}(r,t) * r^{-\gamma(E)}$ [43]. Here, the emissivity profile index is required to be energy-dependent, with $\gamma(E_h) > \gamma(E_s)$, which thus naturally leads to hard lags. Kawamura et al. [44] applied a model based on propagating fluctuations to *Insight*-HXMT observations of MAXI J1820+070. While the original version could not reproduce the data above ~ 10 keV, an updated model including spectral pivoting successfully explained power and phase-lag spectra up to ~ 50 keV. At higher energies, however, the phase-lag spectra remain unexplained, which they suggest is due to the lack of a physical spectral pivoting model.

We used a propagating accretion rate fluctuations model, PROPFLUC [43, 45–48], to characterize the evolution of the hard lags shown in Fig. 5 in terms of physical parameters of the accretion flow. The simulation results suggest that the evolution of the hard lag can be attributed either to variations in the emissivity index difference ($\Delta\gamma$) between energy bands, or to changes in the outer radius of the corona (r_o). For the latter case, the observed softening of the hard lag after epoch 3 spectrum implies a contraction of the corona, consistent with earlier spectral-timing studies. Based on our quantitative estimates, the coronal size increases from $\sim 17R_g$ at epoch 1 to $\sim 50R_g$ at epoch 3, and then gradually decreases to $\sim 32R_g$ by epoch 6. A detailed description of the simulations is provided in the Supplementary Text.

Summary

In this work, the X-ray reverberation mapping measurement was extended to a broadest energy range of ~ 1 –150 keV. We report on the first detection of the Compton hump reverberation feature from an X-ray binary MAXI J1820+070, which accompanies detection of an iron line feature confirming the scenario of X-ray reverberation. Moreover, the lag-energy spectrum aligns with AGN spectra when scaled by mass, providing strong evidence that the accretion flows in AGNs and X-ray binaries are governed by a ubiquitous process.

We also find a clear difference in the reverberation time scales of the iron K emission line and the Compton hump. This may provide the first observational evidence, from a timing perspective, of an ionization gradient in the accretion disk, which highlights the potential value of incorporating such gradients in future spectral modeling efforts.

On longer time scales, the lag-energy spectrum reveals the rapid evolution of the corona during the initial phase of the outburst, suggesting that the coronal properties at this stage differ significantly from those in later stages. This finding highlights the necessity of employing wide-field monitors to capture the very onset of black hole binary outbursts—an accretion phase that has been overlooked. Early detections are crucial for enabling high-quality follow-up spectral, timing, and polarimetric observations with next-generation missions, such as the enhanced X-ray Timing and Polarimetry (eXTP) [49] and Athena [50]. These advancements will enable unprecedented exploration of the physics governing extreme accretion processes during the nascent stages of outburst activity.

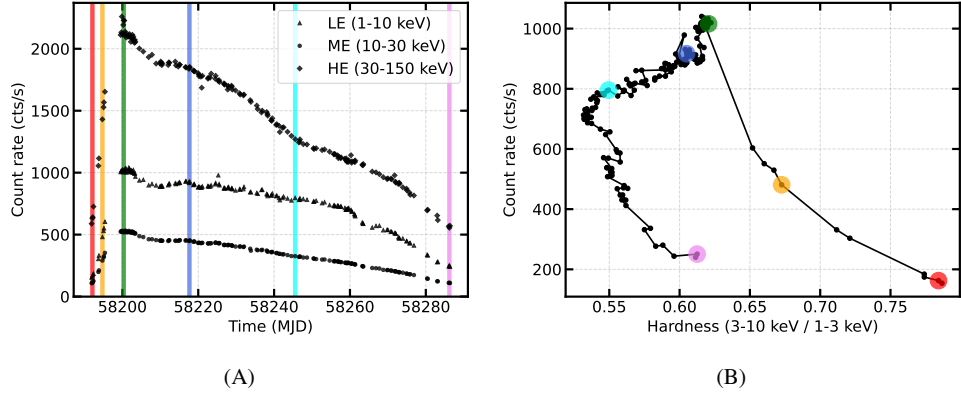


Fig. 1 *Insight-HXMT* lightcurves and corresponding hardness-intensity diagram. (A) *Insight-HXMT* lightcurves (in units of counts per second) of MAXI J1820+070 in HE (27–250 keV), ME (10–30 keV) and LE (1–10 keV) band, in the rising hard state during the outburst ranging from MJD 58192 to 58286. (B) The corresponding hardness-intensity diagram, defined as the total 1–10 keV count rate (in units of counts per second) versus the ratio of hard (3–10 keV) to soft (1–3 keV) count rates. The central times of the six epochs of interest are shown as colored points, corresponding to MJD = 58192, 58194, 58200, 58217, 58245, and 58286.

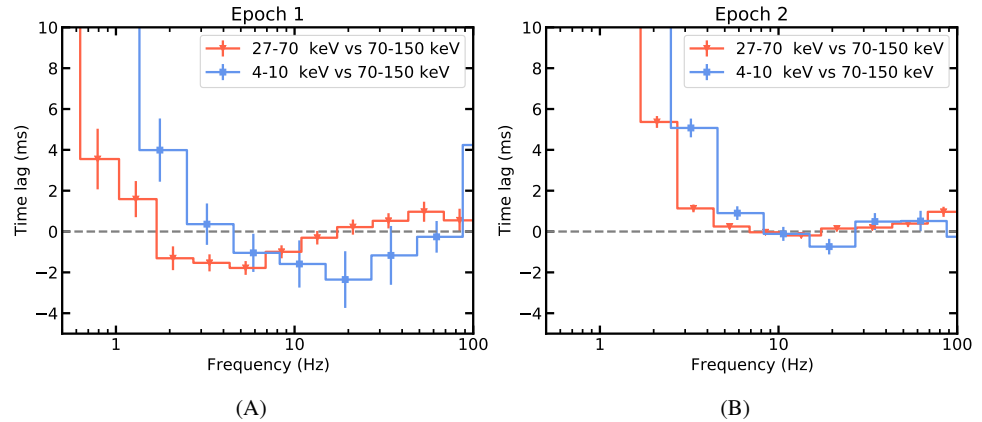


Fig. 2 Lag-frequency spectra of MAXI J1820+070. (A) The 4–10 keV vs. 70–150 keV lag-frequency spectra of the analyzed observations of MAXI J1820+070. (B) The 27–70 keV vs. 70–150 keV lag-frequency spectra. A negative lag suggests that the soft band lags behind the hard ones.

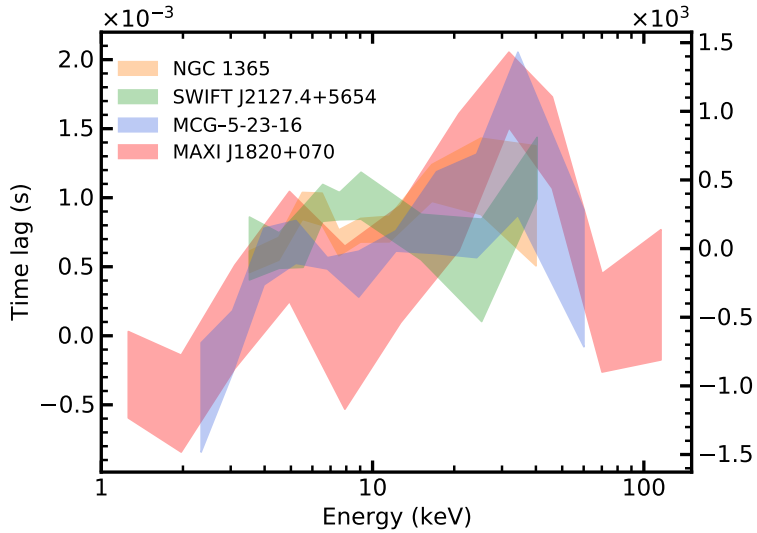


Fig. 3 Comparison of high-frequency lag-energy spectra between AGNs and XRB. The left y-axis displays the lag measurements for XRB MAXI J1820+070 during epoch 1, using a reference band of 1-10 keV, within the 2-60 Hz frequency range where significant high-energy soft lags were observed as depicted in Fig. 2. The right y-axis shows the high-frequency lag-energy spectra for three AGNs: MCG-5-23-16, SWIFT J2127.4+5654, and NGC 1365. These AGNs exhibit detected iron K and Compton hump reverberation lags, highlighting the similarities in the reverberation processes across different scales of black hole systems [24, 25].

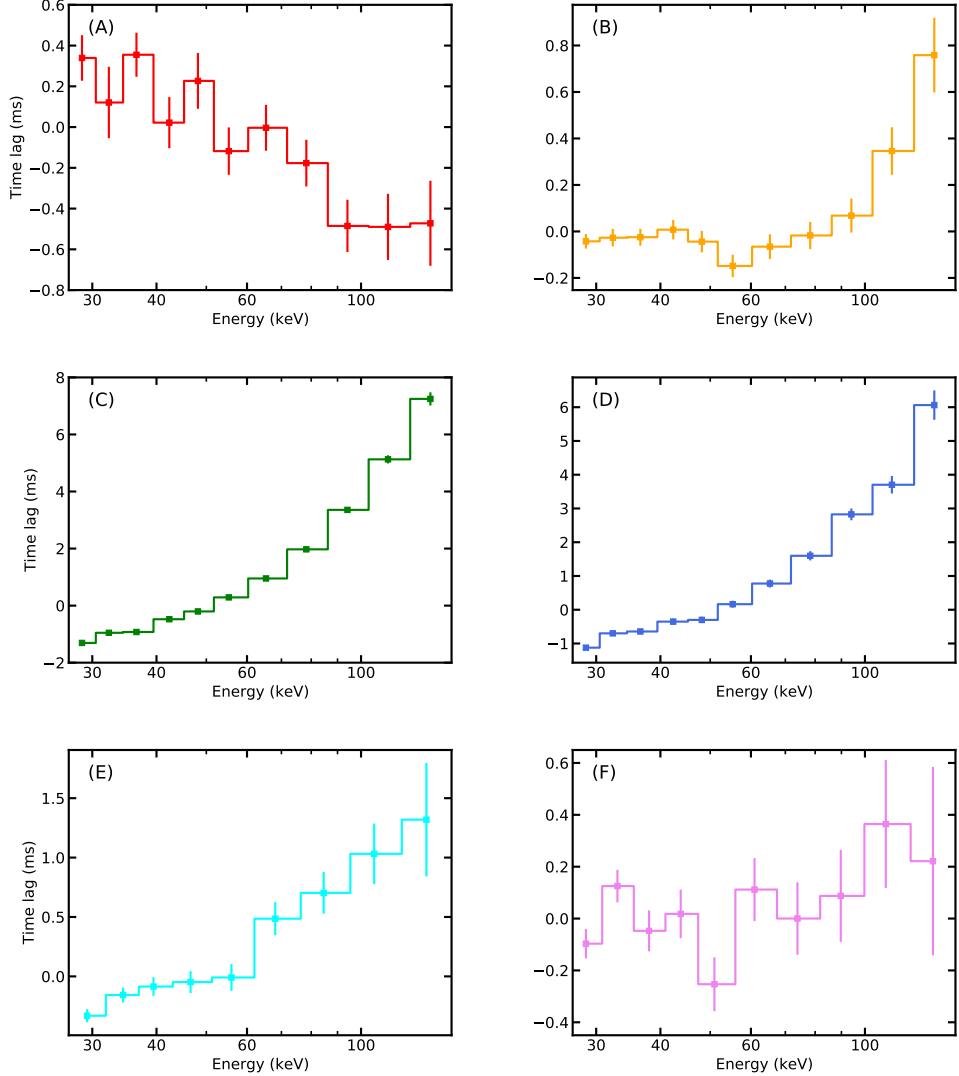


Fig. 4 Evolution of the lag-energy spectra for the six observation epochs. (A)-(F) correspond to the lag-energy spectrum for epochs 1-6, respectively. We take the frequency range of the soft lag which is estimated in the lag-frequency spectra from the *NICER* data (see details in Fig. 2). The reference band is selected as 27-70 keV. The color of each observation matches that in Fig. 1.

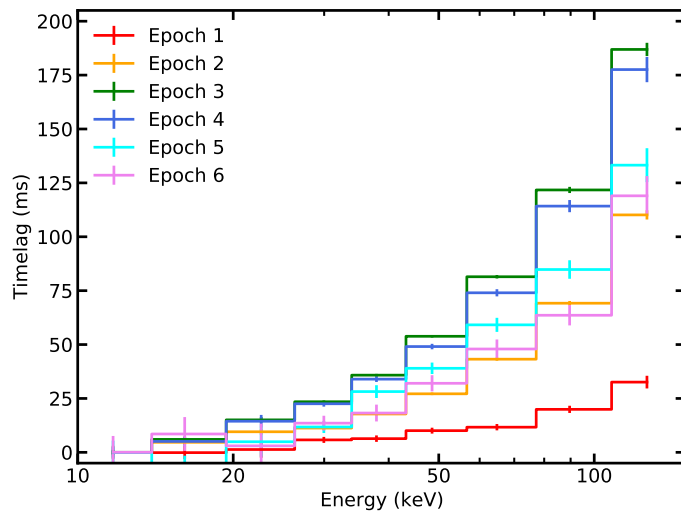


Fig. 5 Low-frequency lag-energy spectra for the six epochs. The frequency range used is 0.1–1 Hz. The reference band is selected as 1–10 keV. The spectra cover the energy range of both ME and HE instruments (10–150 keV). The lags have been shifted such that the lowest-energy lag starts at zero. The color of each observation matches that in Fig. 1.

Table 1 Overview of the observations used in this analysis. This table lists the observation epochs, corresponding dates, Modified Julian Dates (MJD), Observation IDs (ObsID), and observation times in kiloseconds (ks).

epoch	Date	MJD	ObsID	Obs Time (ks)
1	2018-03-14	58192	P0114661001	6.4
2	2018-03-16	58194	P0114661002	34
3	2018-03-22	58200	P0114661003	33
4	2018-04-09	58217	P0114661016	6.3
5	2018-05-07	58245	P0114661040	3.7
6	2018-06-17	58286	P0114661070	2.3

Methods

Data reduction

Insight-HXMT consists of three groups of instruments: High Energy X-ray Telescope (HE, 20-250 keV), Medium Energy X-ray Telescope (ME, 5-30 keV), and Low Energy X-ray Telescope (LE, 1-15 keV). We use the *Insight*-HXMT Data Analysis software (HXMTDAS) v2.05 to analyze the observations. The data are filtered with the following criteria: (1) pointing offset angle $< 0.05^\circ$; (2) elevation angle $> 6^\circ$; (3) the value of the geomagnetic cutoff rigidity > 6 . The backgrounds for HE, ME, and LE are estimated according to the linear correlation between the detectors with a small field of view (FoV) and blind detectors, and the coefficient is the number of nonblind detectors to that of blind detectors. This method is tested by the *Insight*-HXMT background team using blank sky observations and is adopted in the timing analysis of MAXI J1535-571 [51].

Time-lag measurements

X-ray reverberation mapping is a very powerful tool for probing the innermost regions of BHXRBS and AGNs [17, 24, 25, 28, 33, 52]. In this work, we study the X-ray reverberation time delays, which measure the frequency-dependent lags and energy-dependent lags.

Fourier techniques are adopted in this work [6, 14, 53]. The light curves in different energy bands in 0.001s bins. We perform the discrete Fourier transform on each light curve and multiply the Fourier transform of one light curve by the complex conjugate of the Fourier transform of another, which gives the cross-spectrum. The phase of the cross-spectrum thus measures the phase difference between the two light curves. Furthermore, the cross-spectrum is averaged in frequency bins, and this frequency-dependent phase can be converted into a frequency-dependent time lag by dividing by $2\pi f$ where f is the middle frequency of the logarithmic bin. A positive value of the time lag is defined as the hard band light curve being delayed with respect to the soft band.

On the energy dependence of the characteristic phase wrapping frequency

In the first observing epoch, we find that the frequency at which phase wrapping begins, v_0 , is approximately an order of magnitude higher for the 4 – 10 vs 70 – 150 keV lags than it is for the 27 – 70 vs 70 – 150 keV lags. Although the soft lag amplitude itself does not directly indicate the reverberation lag, τ , due to dilution (i.e. both energy bands include contributions from direct and reflected components), it has been shown that the frequency at which the soft lag transitions to a hard lag due to phase wrapping is unaffected by dilution [6, 31, 33, 54]. This implies that $v_0 \propto 1/\tau$ should be independent of the energy bands used to measure the time lag. However, this inference is only true if the emergent reflection spectrum is the same for all disk radii. In reality, the ionization parameter is a strong function of radius due to the radial dependencies of both the irradiating flux and the disk density [55–57]. The ionization parameter strongly influences the strength of the iron line, but not the Compton hump [19], meaning that the iron line essentially originates from a smaller region than the Compton hump does, and thus its associated reverberation lag is smaller, leading to v_0 being higher.

To test this interpretation, we create a new model within the X-ray reverberation mapping software package RELTRANS [56, 58]. The existing RELTRANS models output time lag as a function of energy for a given Fourier frequency range. The new model that we create here, `reltransCpF`, outputs the time lag between two user-defined energy bands as a function of Fourier frequency.

The underlying model is the same as `reltransDCp` [58]. The corona is assumed to be a point-like ‘lamppost’ source a height h above the black hole that illuminates a flat disk with inner and outer radii r_{in} and r_{out} that is observed from an inclination angle i . Other physical parameters are the black hole spin a , the photon index Γ , the ionization parameter $\log \xi$, the iron abundance relative to solar A_{Fe} , the disk density $\log n_e$, the coronal electron temperature kT_e , the black hole mass M , and the boost parameter, which regulates the fraction of the observed flux that is reflected. The coronal spectrum is modeled with the thermal Comptonisation code `nthComp` [59] and the restframe reflection spectrum is modeled using `xillverCp` [19].

Reverberation lags are calculated self-consistently in the assumed geometry, whereas hard lags are created by introducing variability to the photon index $\Gamma(t)$ [60]. The variability in Γ at a Fourier frequency ν is governed by the parameters $\gamma(\nu)$ and $\phi_{AB}(\nu)$, where the former is the variability amplitude relative to that of the normalization, and the latter is the phase lag between the Γ variability and that of the normalization. In the usual RELTRANS models, the user specifies a different value of γ and ϕ_{AB} for each frequency range considered, and these are left as free parameters. For the new frequency-dependent model, we must instead parameterize the frequency dependence of $\gamma(\nu)$ and $\phi_{AB}(\nu)$. We employ the formulae

$$\phi_{AB}(\nu) = \phi_{AB,0} \nu^{-s_{AB}}, \quad \gamma(\nu) = \gamma_0 \nu^{-s_\gamma}. \quad (1)$$

where $\phi_{AB,0}$, s_{AB} , γ_0 and s_γ are model parameters.

We attempt preliminary fits of this new model to the epoch 1 *Insight-HXMT* data. We account for the response matrices of the different instruments used to measure the lags, but ignore interstellar absorption, which is not important at the high photon energies we are considering. Extended Data Fig. 1A shows the result of fitting `reltransCpF` when accounting for the radial dependence of $\log \xi(r)$ by employing a grid of 20 radial zones and assuming a constant disk density. We see that for this model, the frequency at which phase wrapping begins is indeed different for the two different lag spectra: the zero-crossing point is ~ 20 Hz and ~ 30 Hz for the Compton hump and iron line lags, respectively. We note that this difference is smaller than what is seen in the data (~ 20 Hz vs ~ 80 Hz), but the model is consistent with the data within uncertainties. In contrast, Fig. 1B shows the result of fitting the model under the assumption that $\log \xi$ is independent of radius. We see that, as expected, the characteristic phase wrapping frequency is the same for both lag spectra. The parameters of the best fitting model are not believable (e.g. $i \approx 7^\circ$, $M \approx 34 M_\odot$), but after trying many parameter combinations, we reliably find that v_0 can only depend on the energy bands used if a radial $\log \xi$ gradient is employed. In future, we will attempt a formal fit of the epoch 1 data with the `reltransCpF` model.

Simulation of Low-Frequency Hard Lags with the PROPFLUC Model

The PROPFLUC model incorporates fluctuations in the mass accretion rate that propagate through the hot accretion flow, as well as the precession of the entire hot flow induced by frame-dragging effects near the black hole. In this framework, accretion rate fluctuations originate at all radii within the hot flow and travel inward toward the black hole, giving rise to a broadband noise component in the power spectrum. The characteristic timescale of this variability is governed by the local viscous timescale within the flow [11, 61, 62]. Due to the inward propagation of these fluctuations, the variability in the emission from different annuli of the flow is temporally correlated, with time lags corresponding to their respective propagation delays.

Using the PROPFLUC model, we carry out simulations to explore the correlation between the lag due to the propagation of the fluctuations, and emission indices for different corona sizes. The results of these simulations are shown in Extended Data Fig. 4. In the simulations, the outer corona radius (r_o) is a free parameter, while the inner radius (r_i) is kept constant at $4.5 R_g$. We choose an emission index of $\gamma(E_s) = 2.0$ for the reference energy band, with $\Delta\gamma$ representing the difference in the emission indices between the target and reference energy bands. Table 2 provides a detailed overview of the model's parameters.

According to the calculations of the fluctuation model in Extended Data Fig. 4, the weak energy-dependence of the hard lag at epoch 1, which is shown in Fig. 5, could be attributed to two possibilities: (1) a small difference in the emissivity profile between the soft and hard bands $\gamma(E_h) \simeq \gamma(E_s)$; (2) a large difference in the emissivity profile with $\gamma(E_h) \gg \gamma(E_s)$, but a compact corona with small outer radius, e.g., $r_o \leq 20R_g$. As for the first case, the hardening of the hard lag spectrum since epoch 1 would require the increases in the index difference $\Delta\gamma = \gamma(E_h) - \gamma(E_s)$ and/or the size of the corona r_o . Finally, the softening of the hard lag spectrum after epoch 3 (the peak of the count rate) may correspond to the decrease in $\Delta\gamma$ and/or r_o . As for the latter case, the hardening and softening of the hard lag spectrum correspond to an increase and a decrease of r_o , respectively. Indeed, the large $\Delta\gamma$ implies a weak dependence of the hard lag on this parameter. Therefore, a softening of the hard lag spectrum would suggest a contraction of the corona. This is interesting as this discovery is consistent with the conclusions by the *NICER* spectral/timing analysis [17, 28, 33]. Next, we attempt to make a quantitative estimate of the coronal size. Since the dependence of the emissivity profile index γ on energy is unknown, we assume an extreme case for $\Delta\gamma = 6$ and estimate the coronal size using the maximum observed lag amplitude. It should be noted that this assumption may lead to an underestimate of the actual coronal size. The results suggest that the coronal size increases from $\sim 17R_g$ at epoch 1 to $\sim 50R_g$ at epoch 3, and then gradually decreases to $\sim 32R_g$ by epoch 6.

The corona size and its emissivity profile are important properties in picturing the accretion flow near the BH during the initial phase of the outburst. Although it is hard to put constraints on these two quantities in this work, we have shown the advantage of extending the lag measurement to a high energy regime (> 100 keV), which was rarely explored. Moreover, the choice of a hard band (> 70 keV) dominated by the corona Comptonization as the reference band, reveals the unprecedented evolution of the time lag during the outburst. Future studies of broad spectral/timing analysis up to hundreds of keV, possibly combined with X-ray polarization (in the IXPE energy band), are expected to further our knowledge of the accretion process and its evolution during an outburst.

Additional Spectral and Timing Results

Representative X-ray spectra from the selected epochs, together with their data-to-model ratios relative to the best-fitting `cutoffpl` model, are shown in Extended Data Fig. 5. The Iron line and Compton hump inferred from these spectra align well with those seen in the lag–energy spectra, both in terms of energy range and relative strength. In addition, we also present the power spectra extracted from the Compton hump energy band (Extended Data Fig. 6), which further illustrate its contribution to the observed variability.

Data availability

All *Insight*-HXMT data used in this work (Proposal ID: P0114661) are publicly available and can be downloaded from the *Insight*-HXMT website (<http://hxmt.org/> or <http://www.hxmt.cn/>). The NICER datasets analysed during this study are available at NASA’s High Energy Astrophysics Science Archive Research Center (HEASARC; <https://heasarc.gsfc.nasa.gov/>).

Code availability

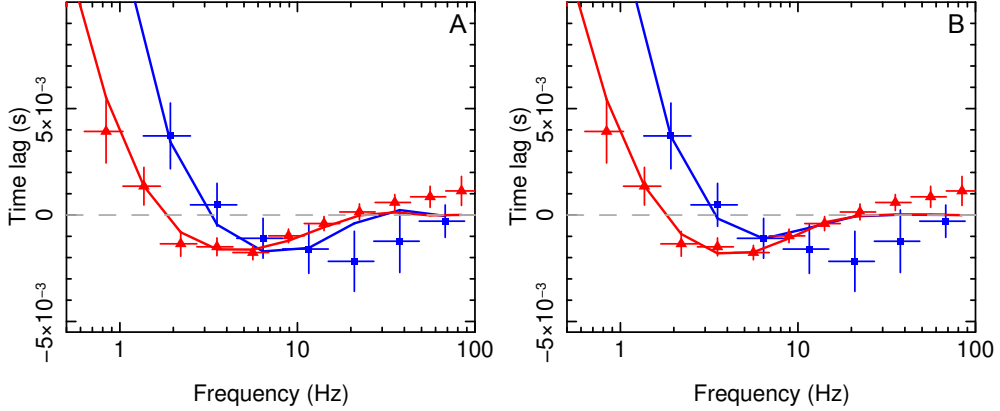
The *Insight*-HXMT data reduction was performed using software available from the *Insight*-HXMT website (<http://www.hxmt.cn/> or <http://hxmt.org/>). The time lag was performed with `Stingray`, a reliable Python library for X-ray timing analysis (see <https://stingray.readthedocs.io/en/latest/index.html>). The model `PROPFLUC` can be downloaded from the website: https://github.com/HEASARC/xspec_localmodels/tree/master/propfluc.

Acknowledgments

B. Y. is supported by NSFC grants 12322307, 12361131579, 12273026; by the National Program on Key Research and Development Project 2021YFA0718500; Xiaomi Foundation / Xiaomi Young Talents Program. W. Y. acknowledges financial support from the Sino-German (CSC–DAAD) Postdoc Scholarship Program (No. 57718047). A. I. acknowledges support from the Royal Society. B.D.M. acknowledges support via a Ramón y Cajal Fellowship (RYC2018-025950-I), the Spanish MINECO grants PID2023-148661NB-I00, PID2022-136828NB-C44, and the AGAUR/Generalitat de Catalunya grant SGR-386/2021. J.-L. Q. acknowledges support from the grant U2031205. Z.-H. Z. acknowledges support from the National Natural Science Foundation of China under Grants Nos. 12021003 and 12433001.

Author contributions:

B.Y. initiated the project, specifically proposing data analysis and model interpretation, and took the lead in manuscript writing. W. Y. led the timing analysis and contributed to the text writing. A.I. led the interpretation of the Frequency-dependent time lags, and contributed to the writing of the text. B. D. contributed to the model discussion and the writing of the text. J.-L. Q., Z.-H. Z, and A.S. contributed to the model discussion. All the authors joined in the modification of the text at all stages.



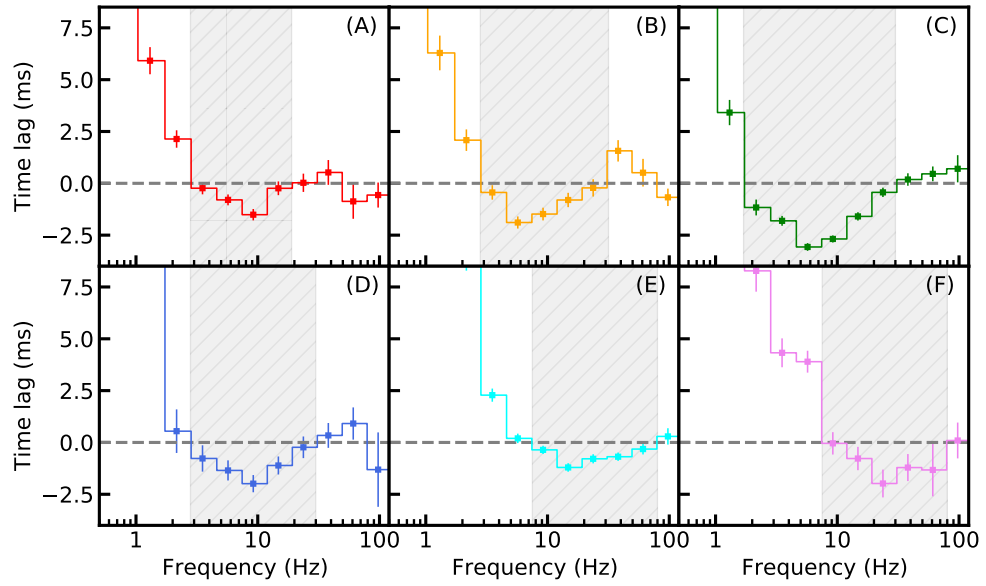
Extended Data Fig. 1 Example fits to the epoch 1 lag spectrum with a reverberation model. We use a new model in the RELTRANS package to model the epoch 1 lag vs frequency spectra for 4 – 10 keV vs 70 – 150 keV (blue squares) and 27 – 70 keV vs 70 – 150 keV (red triangles). The data are identical to those shown in Fig. 2. (A): The model accounts for a radial ionization gradient, enabling phase wrapping to begin at a different frequency for the two lag spectra. (B): The model assumes a constant disk ionization parameter, meaning that phase wrapping always begins at the same frequency.

Table 2 Parameters in PROPFLUC. This table details the parameters used in the PROPFLUC model, including their descriptions and corresponding values.

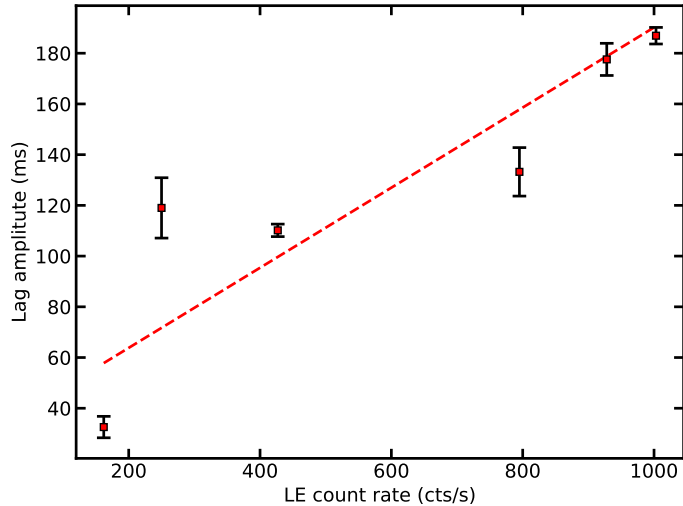
Parameter	Description	Value
Σ_0	Normalisation of surface density profile	10
r_{bw}	Bending wave radius	7
κ	Surface density profile parameter	3
λ	Surface density profile parameter	0.9
ζ	Surface density profile parameter	0
F_{var}	Fractional variability per decade in radius	0.3
r_i	Inner radius of the flow	4.5
M	BH mass in Solar masses	10
a	Dimensionless spin parameter	0.998
N_{dec}	Number of rings per decade in radius	35

Competing interests:

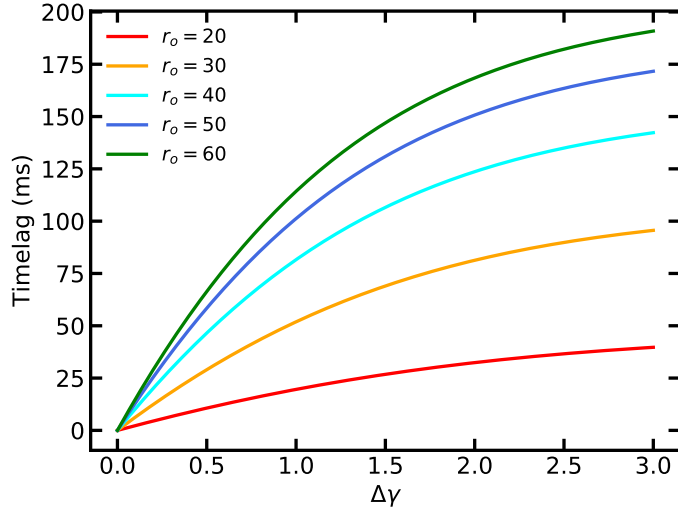
There are no competing interests to declare.



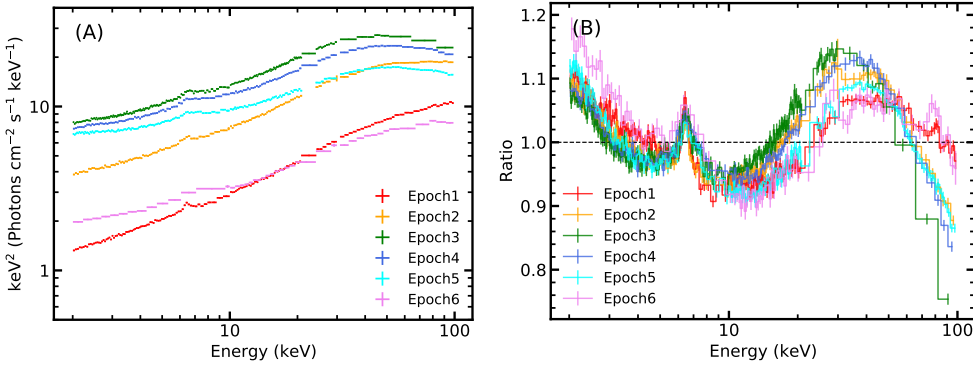
Extended Data Fig. 2 The *NICER* lag-frequency spectra measured between 0.5–1 keV and 2–5 keV. (A)–(F) correspond to quasi-simultaneous *NICER* observations for epochs 1–6, respectively. The shaded regions indicate where a soft reverberation lag is detected, with these frequency ranges employed to calculate the lag-energy spectra in Fig. 4.



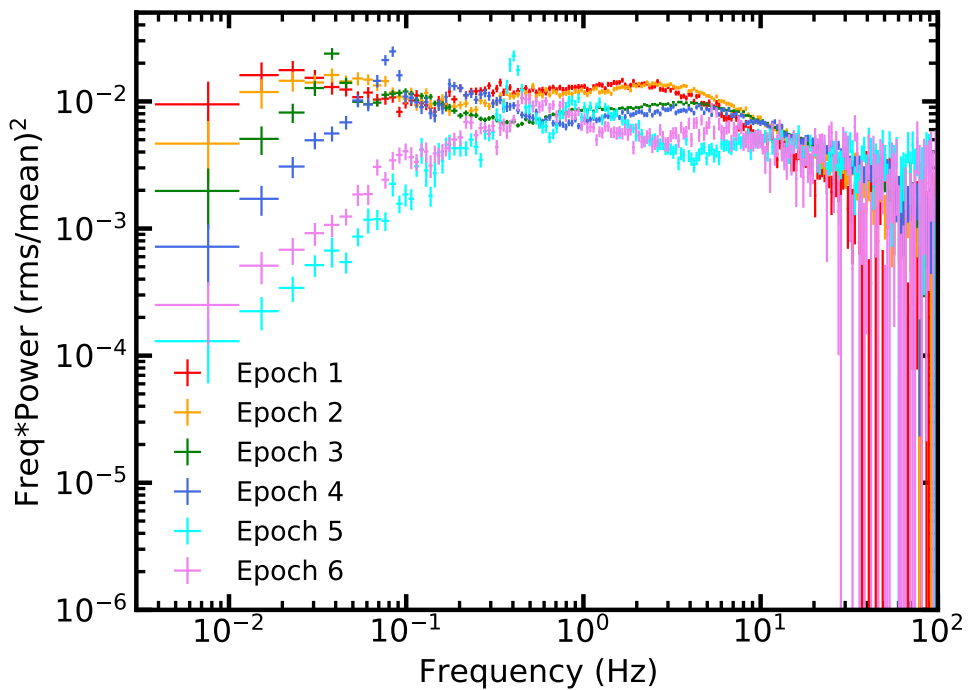
Extended Data Fig. 3 The amplitude of low-frequency hard lags as a function of LE count rates. The red dashed line represents the best linear fit.



Extended Data Fig. 4 Simulated low-frequency (0.1–1 Hz) lag spectra using the PROPFLUC model. The low-frequency (0.1–1 Hz) lag spectra simulated using the propagating mass accretion rate fluctuations model PROPFLUC. Most model parameters were fixed, with only the emissivity index and the outer radius of the corona varying.



Extended Data Fig. 5 *Insight-HXMT* X-ray spectra from the selected observational epochs. (A) *Insight-HXMT* X-ray spectra of MAXI J1820+070 for six epochs. (B) Data-to-model ratios with respect to the best-fit `cutoffpl` model, highlighting the Fe-K line and Compton hump relative to the continuum.



Extended Data Fig. 6 Power spectra from the Compton hump band. *Insight-HXMT* power spectra extracted from the 27–70 keV band for the six epochs.

References

- [1] Lasota, J.-P.: The disc instability model of dwarf novae and low-mass X-ray binary transients. *New Astronomy Reviews* **45**(7), 449–508 (2001) [https://doi.org/10.1016/S1387-6473\(01\)00112-9](https://doi.org/10.1016/S1387-6473(01)00112-9) [arXiv:astro-ph/0102072](https://arxiv.org/abs/astro-ph/0102072) [astro-ph]
- [2] Wilkinson, T., Uttley, P.: Accretion disc variability in the hard state of black hole x-ray binaries. *Monthly Notices of the Royal Astronomical Society* **397**(2), 666–676 (2009)
- [3] Uttley, P., McHardy, I.M., Papadakis, I.E.: Measuring the broad-band power spectra of active galactic nuclei with RXTE. *Monthly Notices of the Royal Astronomical Society* **332**(1), 231–250 (2002) <https://doi.org/10.1046/j.1365-8711.2002.05298.x> [arXiv:astro-ph/0201134](https://arxiv.org/abs/astro-ph/0201134) [astro-ph]
- [4] Uttley, P., Wilkinson, T., Cassatella, P., Wilms, J., Pottschmidt, K., Hanke, M., Böck, M.: The causal connection between disc and power-law variability in hard state black hole X-ray binaries. *Monthly Notices of the Royal Astronomical Society* **414**(1), 60–64 (2011) <https://doi.org/10.1111/j.1745-3933.2011.01056.x> [arXiv:1104.0634](https://arxiv.org/abs/1104.0634) [astro-ph.HE]
- [5] Cassatella, P., Uttley, P., Wilms, J., Poutanen, J.: Joint spectral-timing modelling of the hard lags in gx 339- 4: constraints on reflection models. *Monthly Notices of the Royal Astronomical Society* **422**(3), 2407–2416 (2012)
- [6] Uttley, P., Cackett, E.M., Fabian, A.C., Kara, E., Wilkins, D.R.: X-ray reverberation around accreting black holes. *The Astronomy and Astrophysics Review* **22**, 72 (2014) <https://doi.org/10.1007/s00159-014-0072-0> [arXiv:1405.6575](https://arxiv.org/abs/1405.6575) [astro-ph.HE]
- [7] Méndez, M., Karpouzas, K., García, F., Zhang, L., Zhang, Y., Belloni, T.M., Altamirano, D.: Coupling between the accreting corona and the relativistic jet in the microquasar grs 1915+ 105. *Nature Astronomy* **6**(5), 577–583 (2022)
- [8] Méndez, M., Karpouzas, K., García, F., Zhang, L., Zhang, Y., Belloni, T.M., Altamirano, D.: Coupling between the accreting corona and the relativistic jet in the microquasar GRS 1915+105. *Nature Astronomy* **6**, 577–583 (2022) <https://doi.org/10.1038/s41550-022-01617-y> [arXiv:2203.02963](https://arxiv.org/abs/2203.02963) [astro-ph.HE]
- [9] Uttley, P., Malzac, J.: Large and complex x-ray time lags from black hole accretion discs with compact inner coronae. *Monthly Notices of the Royal Astronomical Society* **536**(4), 3284–3307 (2025)
- [10] Kotov, O., Churazov, E., Gilfanov, M.: On the X-ray time-lags in the black hole candidates. *Monthly Notices of the Royal Astronomical Society* **327**(3), 799–807 (2001) <https://doi.org/10.1046/j.1365-8711.2001.04769.x> [arXiv:astro-ph/0103115](https://arxiv.org/abs/astro-ph/0103115) [astro-ph]
- [11] Arévalo, P., Uttley, P.: Investigating a fluctuating-accretion model for the spectral-timing

properties of accreting black hole systems. *Monthly Notices of the Royal Astronomical Society* **367**(2), 801–814 (2006) <https://doi.org/10.1111/j.1365-2966.2006.09989.x> [arXiv:astro-ph/0512394](https://arxiv.org/abs/astro-ph/0512394) [astro-ph]

[12] Kylafis, N., Papadakis, I., Reig, P., Giannios, D., Pooley, G.: A jet model for galactic black-hole x-ray sources: some constraining correlations. *Astronomy & Astrophysics* **489**(2), 481–487 (2008)

[13] Balbus, S.A., Hawley, J.F.: Instability, turbulence, and enhanced transport in accretion disks. *Reviews of modern physics* **70**(1), 1 (1998)

[14] Nowak, M.A., Vaughan, B.A., Wilms, J., Dove, J.B., Begelman, M.C.: Rossi X-Ray Timing Explorer Observation of Cygnus X-1. II. Timing Analysis. *The Astrophysical Journal* **510**(2), 874–891 (1999) <https://doi.org/10.1086/306610> [arXiv:astro-ph/9807278](https://arxiv.org/abs/astro-ph/9807278) [astro-ph]

[15] De Marco, B., Ponti, G., Muñoz-Darias, T., Nandra, K.: Tracing the Reverberation Lag in the Hard State of Black Hole X-Ray Binaries. *The Astrophysical Journal* **814**(1), 50 (2015) <https://doi.org/10.1088/0004-637X/814/1/50> [arXiv:1510.02798](https://arxiv.org/abs/1510.02798) [astro-ph.HE]

[16] De Marco, B., Ponti, G., Petrucci, P., Clavel, M., Corbel, S., Belmont, R., Chakravorty, S., Coriat, M., Drappeau, S., Ferreira, J., *et al.*: Evolution of the reverberation lag in gx 339-4 at the end of an outburst. *Monthly Notices of the Royal Astronomical Society* **471**(2), 1475–1487 (2017)

[17] Kara, E., Steiner, J.F., Fabian, A.C., Cackett, E.M., Uttley, P., Remillard, R.A., Gendreau, K.C., Arzoumanian, Z., Altamirano, D., Eikenberry, S., Enoto, T., Homan, J., Neilsen, J., Stevens, A.L.: The corona contracts in a black-hole transient. *Nature* **565**(7738), 198–201 (2019) <https://doi.org/10.1038/s41586-018-0803-x> [arXiv:1901.03877](https://arxiv.org/abs/1901.03877) [astro-ph.HE]

[18] Fabian, A., Ross, R.: X-ray reflection. *Space science reviews* **157**, 167–176 (2010)

[19] García, J., Dauser, T., Reynolds, C.S., Kallman, T.R., McClintock, J.E., Wilms, J., Eikmann, W.: X-Ray Reflected Spectra from Accretion Disk Models. III. A Complete Grid of Ionized Reflection Calculations. *The Astrophysical Journal* **768**(2), 146 (2013) <https://doi.org/10.1088/0004-637X/768/2/146> [arXiv:1303.2112](https://arxiv.org/abs/1303.2112) [astro-ph.HE]

[20] Dauser, T., García, J., Wilms, J.: Relativistic reflection: Review and recent developments in modeling. *Astronomische Nachrichten* **337**(4-5), 362–367 (2016)

[21] Zdziarski, A.A., Gierliński, M.: Radiative Processes, Spectral States and Variability of Black-Hole Binaries. *Progress of Theoretical Physics Supplement* **155**, 99–119 (2004) <https://doi.org/10.1143/PTPS.155.99> [arXiv:astro-ph/0403683](https://arxiv.org/abs/astro-ph/0403683) [astro-ph]

[22] You, B., Tuo, Y., Li, C., Wang, W., Zhang, S.-N., Zhang, S., Ge, M., Luo, C., Liu, B., Yuan, W., Dai, Z., Liu, J., Qiao, E., Jin, C., Liu, Z., Czerny, B., Wu, Q., Bu, Q., Cai,

C., Cao, X., Chang, Z., Chen, G., Chen, L., Chen, T., Chen, Y., Chen, Y., Chen, Y., Cui, W., Cui, W., Deng, J., Dong, Y., Du, Y., Fu, M., Gao, G., Gao, H., Gao, M., Gu, Y., Guan, J., Guo, C., Han, D., Huang, Y., Huo, J., Jia, S., Jiang, L., Jiang, W., Jin, J., Jin, Y., Kong, L., Li, B., Li, C., Li, G., Li, M., Li, T., Li, W., Li, X., Li, X., Li, X., Li, Y., Li, Z., Liang, X., Liao, J., Liu, C., Liu, G., Liu, H., Liu, X., Liu, Y., Lu, B., Lu, F., Lu, X., Luo, Q., Luo, T., Ma, X., Meng, B., Nang, Y., Nie, J., Ou, G., Qu, J., Sai, N., Shang, R., Song, L., Song, X., Sun, L., Tan, Y., Tao, L., Wang, C., Wang, G., Wang, J., Wang, L., Wang, W., Wang, Y., Wen, X., Wu, B., Wu, B., Wu, M., Xiao, G., Xiao, S., Xiong, S., Xu, Y., Yang, J., Yang, S., Yang, Y., Yi, Q., Yin, Q., You, Y., Zhang, A., Zhang, C., Zhang, F., Zhang, H., Zhang, J., Zhang, T., Zhang, W., Zhang, W., Zhang, W., Zhang, Y., Zhang, Y., Zhang, Y., Zhang, Z., Zhao, H., Zhao, X., Zheng, S., Zhou, D., Zhou, J., Zhu, Y., Zhu, Y.: Insight-HXMT observations of jet-like corona in a black hole X-ray binary MAXI J1820+070. *Nature Communications* **12**, 1025 (2021) <https://doi.org/10.1038/s41467-021-21169-5> arXiv:2102.07602 [astro-ph.HE]

[23] Fabian, A.C., Zoghbi, A., Ross, R.R., Uttley, P., Gallo, L.C., Brandt, W.N., Blustin, A.J., Boller, T., Caballero-Garcia, M.D., Larsson, J., Miller, J.M., Miniutti, G., Ponti, G., Reis, R.C., Reynolds, C.S., Tanaka, Y., Young, A.J.: Broad line emission from iron K- and L-shell transitions in the active galaxy 1H0707-495. *Nature* **459**(7246), 540–542 (2009) <https://doi.org/10.1038/nature08007>

[24] Zoghbi, A., Cackett, E., Reynolds, C., Kara, E., Harrison, F., Fabian, A., Lohfink, A., Matt, G., Balokovic, M., Boggs, S., *et al.*: Observations of MCG-5-23-16 with Suzaku, XMM-Newton and NuSTAR: Disk tomography and Compton hump reverberation. *The Astrophysical Journal* **789**(1), 56 (2014)

[25] Kara, E., Zoghbi, A., Marinucci, A., Walton, D.J., Fabian, A.C., Risaliti, G., Boggs, S.E., Christensen, F.E., Fuerst, F., Hailey, C.J., Harrison, F.A., Matt, G., Parker, M.L., Reynolds, C.S., Stern, D., Zhang, W.W.: Iron K and Compton hump reverberation in Swift J2127.4+5654 and NGC 1365 revealed by NuSTAR and XMM-Newton. *Monthly Notices of the Royal Astronomical Society* **446**(1), 737–749 (2015) <https://doi.org/10.1093/mnras/stu2136> arXiv:1410.3357 [astro-ph.HE]

[26] McHardy, I.M., Koerding, E., Knigge, C., Uttley, P., Fender, R.: Active galactic nuclei as scaled-up galactic black holes. *Nature* **444**(7120), 730–732 (2006)

[27] Arévalo, P., Papadakis, I., Uttley, P., McHardy, I., Brinkmann, W.: Spectral-timing evidence for a very high state in the narrow-line Seyfert 1 galaxy 564. *Monthly Notices of the Royal Astronomical Society* **372**(1), 401–409 (2006)

[28] Wang, J., Kara, E., Lucchini, M., Ingram, A., van der Klis, M., Mastroserio, G., García, J.A., Dauser, T., Connors, R., Fabian, A.C., Steiner, J.F., Remillard, R.A., Cackett, E.M., Uttley, P., Altamirano, D.: The NICER “Reverberation Machine”: A Systematic Study of Time Lags in Black Hole X-Ray Binaries. *The Astrophysical Journal* **930**(1), 18 (2022) <https://doi.org/10.3847/1538-4357/ac6262> arXiv:2205.00928 [astro-ph.HE]

[29] Zhang, S., Lu, F.J., Zhang, S.N., Li, T.P.: Introduction to the hard x-ray modulation

telescope. In: Takahashi, T., den Herder, J.-W.A., Bautz, M. (eds.) Space Telescopes and Instrumentation 2014: Ultraviolet to Gamma Ray. Society of Photo-Optical Instrumentation Engineers (SPIE) Conference Series, vol. 9144, p. 914421 (2014). <https://doi.org/10.1117/12.2054144>

[30] You, B., Cao, X., Yan, Z., Hameury, J.-M., Czerny, B., Wu, Y., Xia, T., Sikora, M., Zhang, S.-N., Du, P., Zyczyński, P.T.: Observations of a black hole x-ray binary indicate formation of a magnetically arrested disk. *Science* **381**(6661), 961–964 (2023) <https://doi.org/10.1126/science.abo4504> [arXiv:2309.00200](https://arxiv.org/abs/2309.00200) [astro-ph.HE]

[31] Wilkins, D.R., Fabian, A.C.: The origin of the lag spectra observed in AGN: Reverberation and the propagation of X-ray source fluctuations. *Monthly Notices of the Royal Astronomical Society* **430**(1), 247–258 (2013) <https://doi.org/10.1093/mnras/sts591> [arXiv:1212.2213](https://arxiv.org/abs/1212.2213) [astro-ph.HE]

[32] Mahmoud, R.D., Done, C., De Marco, B.: Reverberation reveals the truncated disc in the hard state of gx 339-4. *Monthly Notices of the Royal Astronomical Society* **486**(2), 2137–2152 (2019)

[33] De Marco, B., Zdziarski, A.A., Ponti, G., Migliori, G., Belloni, T.M., Segovia Otero, A., Dziełak, M.A., Lai, E.V.: The inner flow geometry in MAXI J1820+070 during hard and hard-intermediate states. *Astronomy and Astrophysics* **654**, 14 (2021) <https://doi.org/10.1051/0004-6361/202140567> [arXiv:2102.07811](https://arxiv.org/abs/2102.07811) [astro-ph.HE]

[34] Wandel, A., Mushotzky, R.F.: Observational determination of the masses of active galactic nuclei. *Astrophysical Journal, Part 2-Letters to the Editor* (ISSN 0004-637X), vol. 306, July 15, 1986, p. L61-L65. **306**, 61–65 (1986)

[35] Marconi, A., Hunt, L.K.: The relation between black hole mass, bulge mass, and near-infrared luminosity. *The Astrophysical Journal* **589**(1), 21 (2003)

[36] Malizia, A., Bassani, L., Bird, A., Landi, R., Masetti, N., De Rosa, A., Panessa, F., Molina, M., Dean, A., Perri, M., *et al.*: First high-energy observations of narrow-line Seyfert 1s with integral/ibis. *Monthly Notices of the Royal Astronomical Society* **389**(3), 1360–1366 (2008)

[37] Ponti, G., Papadakis, I., Bianchi, S., Guainazzi, M., Matt, G., Uttley, P., Bonilla, N.: Caixa: a catalogue of agn in the xmm-newton archive-iii. excess variance analysis. *Astronomy & Astrophysics* **542**, 83 (2012)

[38] Emmanoulopoulos, D., Papadakis, I., Dovčiak, M., McHardy, I.: General relativistic modelling of the negative reverberation x-ray time delays in agn. *Monthly Notices of the Royal Astronomical Society* **439**(4), 3931–3950 (2014)

[39] Lyubarskii, Y.E.: Flicker noise in accretion discs. *Monthly Notices of the Royal Astronomical Society* **292**(3), 679–685 (1997)

[40] Nowak, M.A., Vaughan, B.A., Wilms, J., Dove, J.B., Begelman, M.C.: Rossi X-Ray Timing Explorer Observation of Cygnus X-1. II. Timing Analysis. *The Astrophysical Journal* **510**(2), 874–891 (1999) <https://doi.org/10.1086/306610> arXiv:astro-ph/9807278 [astro-ph]

[41] Pottschmidt, K., Wilms, J., Nowak, M.A., Heindl, W.A., Smith, D.M., Staubert, R.: Temporal evolution of X-ray lags in Cygnus X-1. *Astronomy and Astrophysics* **357**, 17–20 (2000) <https://doi.org/10.48550/arXiv.astro-ph/0004018> arXiv:astro-ph/0004018 [astro-ph]

[42] Wang, Y., Ji, L., Zhang, S., Méndez, M., Qu, J., Maggi, P., Ge, M., Qiao, E., Tao, L., Zhang, S., *et al.*: The evolution of the broadband temporal features observed in the black-hole transient maxi j1820+ 070 with insight-hxmt. *The Astrophysical Journal* **896**(1), 33 (2020)

[43] Ingram, A., Done, C.: Modelling variability in black hole binaries: linking simulations to observations. *Monthly Notices of the Royal Astronomical Society* **419**(3), 2369–2378 (2012) <https://doi.org/10.1111/j.1365-2966.2011.19885.x> arXiv:1108.0789 [astro-ph.HE]

[44] Kawamura, T., Done, C., Axelsson, M., Takahashi, T.: Maxi j1820+ 070 x-ray spectral-timing reveals the nature of the accretion flow in black hole binaries. *Monthly Notices of the Royal Astronomical Society* **519**(3), 4434–4453 (2023)

[45] Ingram, A., Done, C.: A physical model for the continuum variability and quasi-periodic oscillation in accreting black holes. *Monthly Notices of the Royal Astronomical Society* **415**(3), 2323–2335 (2011) <https://doi.org/10.1111/j.1365-2966.2011.18860.x> arXiv:1101.2336 [astro-ph.SR]

[46] Ingram, A., van der Klis, M.: An exact analytic treatment of propagating mass accretion rate fluctuations in X-ray binaries. *Monthly Notices of the Royal Astronomical Society* **434**(2), 1476–1485 (2013) <https://doi.org/10.1093/mnras/stt1107> arXiv:1306.3823 [astro-ph.HE]

[47] Rapisarda, S., Ingram, A., van der Klis, M.: Evolution of the hot flow of MAXI J1543-564. *Monthly Notices of the Royal Astronomical Society* **440**(3), 2882–2893 (2014) <https://doi.org/10.1093/mnras/stu461> arXiv:1403.2308 [astro-ph.HE]

[48] Rapisarda, S., Ingram, A., Kalamkar, M., van der Klis, M.: Modelling the cross-spectral variability of the black hole binary MAXI J1659-152 with propagating accretion rate fluctuations. *Monthly Notices of the Royal Astronomical Society* **462**(4), 4078–4093 (2016) <https://doi.org/10.1093/mnras/stw1878> arXiv:1607.08178 [astro-ph.HE]

[49] De Rosa, A., Uttley, P., Gou, L., Liu, Y., Bambi, C., Barret, D., Belloni, T., Berti, E., Bianchi, S., Caiazzo, I., Casella, P., Feroci, M., Ferrari, V., Gualtieri, L., Heyl, J., Ingram, A., Karas, V., Lu, F., Luo, B., Matt, G., Motta, S., Neilsen, J., Pani, P., Santangelo, A., Shu, X., Wang, J., Wang, J.-M., Xue, Y., Xu, Y., Yuan, W., Yuan, Y.,

Zhang, S.-N., Zhang, S., Agudo, I., Amati, L., Andersson, N., Baglio, C., Bakala, P., Baykal, A., Bhattacharyya, S., Bombaci, I., Bucciantini, N., Capitanio, F., Ciolfi, R., Cui, W.K., D’Ammando, F., Dauser, T., Del Santo, M., De Marco, B., Di Salvo, T., Done, C., Dovčiak, M., Fabian, A.C., Falanga, M., Gambino, A.F., Gendre, B., Grinberg, V., Heger, A., Homan, J., Iaria, R., Jiang, J., Jin, C., Koerding, E., Linares, M., Liu, Z., Maccarone, T.J., Malzac, J., Manousakis, A., Marin, F., Marinucci, A., Mehdipour, M., Méndez, M., Migliari, S., Miller, C., Miniutti, G., Nardini, E., O’Brien, P.T., Osborne, J.P., Petrucci, P.O., Possenti, A., Riggio, A., Rodriguez, J., Sanna, A., Shao, L., Sobolewska, M., Sramkova, E., Stevens, A.L., Stiele, H., Stratta, G., Stuchlik, Z., Svoboda, J., Tamburini, F., Tauris, T.M., Tombesi, F., Torok, G., Urbanec, M., Vincent, F., Wu, Q., Yuan, F., in’t Zand, J.J.M., Zdziarski, A.A., Zhou, X.: Accretion in strong field gravity with eXTP. *Science China Physics, Mechanics, and Astronomy* **62**(2), 29504 (2019) <https://doi.org/10.1007/s11433-018-9297-0> arXiv:1812.04022 [astro-ph.HE]

[50] Nandra, K., Barret, D., Barcons, X., Fabian, A., den Herder, J.-W., Piro, L., Watson, M., Adami, C., Aird, J., Afonso, J.M., Alexander, D., Argiroffi, C., Amati, L., Arnaud, M., Atteia, J.-L., Audard, M., Badenes, C., Ballet, J., Ballo, L., Bamba, A., Bhardwaj, A., Stefano Battistelli, E., Becker, W., De Becker, M., Behar, E., Bianchi, S., Biffi, V., Břízan, L., Bocchino, F., Bogdanov, S., Boirin, L., Boller, T., Borgani, S., Borm, K., Bouché, N., Bourdin, H., Bower, R., Braito, V., Branchini, E., Branduardi-Raymont, G., Bregman, J., Brenneman, L., Brightman, M., Brüggen, M., Buchner, J., Bulbul, E., Brusa, M., Bursa, M., Caccianiga, A., Cackett, E., Campana, S., Cappelluti, N., Cappi, M., Carrera, F., Ceballos, M., Christensen, F., Chu, Y.-H., Churazov, E., Clerc, N., Corbel, S., Corral, A., Comastri, A., Costantini, E., Croston, J., Dadina, M., D’Ai, A., Decourchelle, A., Della Ceca, R., Dennerl, K., Dolag, K., Done, C., Dovciak, M., Drake, J., Eckert, D., Edge, A., Ettori, S., Ezoe, Y., Feigelson, E., Fender, R., Feruglio, C., Finoguenov, A., Fiore, F., Galeazzi, M., Gallagher, S., Gandhi, P., Gaspari, M., Gastaldello, F., Georgakakis, A., Georgantopoulos, I., Gilfanov, M., Gitti, M., Gladstone, R., Goosmann, R., Gosset, E., Grossi, N., Guedel, M., Guerrero, M., Haberl, F., Hardcastle, M., Heinz, S., Alonso Herrero, A., Hervé, A., Holmstrom, M., Iwasawa, K., Jonker, P., Kaastra, J., Kara, E., Karas, V., Kastner, J., King, A., Kosenko, D., Koutroumpa, D., Kraft, R., Kreykenbohm, I., Lallement, R., Lanzuisi, G., Lee, J., Lemoine-Goumard, M., Lobban, A., Lodato, G., Lovisari, L., Lotti, S., McCharthy, I., McNamara, B., Maggio, A., Maiolino, R., De Marco, B., de Martino, D., Mateos, S., Matt, G., Maughan, B., Mazzotta, P., Mendez, M., Merloni, A., Micela, G., Miceli, M., Mignani, R., Miller, J., Miniutti, G., Molendi, S., Montez, R., Moretti, A., Motch, C., Nazé, Y., Nevalainen, J., Nicastro, F., Nulsen, P., Ohashi, T., O’Brien, P., Osborne, J., Oskinova, L., Pacaud, F., Paerels, F., Page, M., Papadakis, I., Pareschi, G., Petre, R., Petrucci, P.-O., Piconcelli, E., Pillitteri, I., Pinto, C., de Plaa, J., Pointecouteau, E., Ponman, T., Ponti, G., Porquet, D., Pounds, K., Pratt, G., Predehl, P., Proga, D., Psaltis, D., Rafferty, D., Ramos-Caja, M., Ranalli, P., Rasia, E., Rau, A., Rauw, G., Rea, N., Read, A., Reeves, J., Reiprich, T., Renaud, M., Reynolds, C., Risaliti, G., Rodriguez, J., Rodriguez Hidalgo, P., Roncarelli, M., Rosario, D., Rossetti, M., Rozanska, A., Rovilos, E., Salvaterra, R., Salvato, M., Di Salvo, T., Sanders, J., Sanz-Forcada, J., Schawinski, K., Schaye, J., Schwope, A., Sciortino, S.: The Hot and Energetic Universe: A White Paper presenting the science theme motivating the Athena+ mission. arXiv

e-prints, 1306–2307 (2013) <https://doi.org/10.48550/arXiv.1306.2307> arXiv:1306.2307 [astro-ph.HE]

- [51] Huang, Y., Qu, J.L., Zhang, S.N., Bu, Q.C., Chen, Y.P., Tao, L., Zhang, S., Lu, F.J., Li, T.P., Song, L.M., Xu, Y.P., Cao, X.L., Chen, Y., Liu, C.Z., Chang, H.-K., Yu, W.F., Weng, S.S., Hou, X., Kong, A.K.H., Xie, F.G., Zhang, G.B., ZHOU, J.F., Chang, Z., Chen, G., Chen, L., Chen, T.X., Chen, Y.B., Cui, W., Cui, W.W., Deng, J.K., Dong, Y.W., Du, Y.Y., Fu, M.X., Gao, G.H., Gao, H., Gao, M., Ge, M.Y., Gu, Y.D., Guan, J., Gungor, C., Guo, C.C., Han, D.W., Hu, W., Huo, J., Ji, J.F., Jia, S.M., Jiang, L.H., Jiang, W.C., Jin, J., Jin, Y.J., Li, B., Li, C.K., Li, G., Li, M.S., Li, W., Li, X., Li, X.B., Li, X.F., Li, Y.G., Li, Z.J., Li, Z.W., Liang, X.H., Liao, J.Y., Liu, G.Q., Liu, H.W., Liu, S.Z., Liu, X.J., Liu, Y., Liu, Y.N., Lu, B., Lu, X.F., Luo, T., Ma, X., Meng, B., Nang, Y., Nie, J.Y., Ou, G., Sai, N., Shang, R.C., Sun, L., Tan, Y., Tao, W., Tuo, Y.L., Wang, G.F., Wang, H.Y., Wang, J., Wang, W.S., Wang, Y.S., Wen, X.Y., Wu, B.B., Wu, M., Xiao, G.C., Xiong, S.L., Xu, H., Yan, L.L., Yang, J.W., Yang, S., Yang, Y.J., Zhang, A.M., Zhang, C.L., Zhang, C.M., Zhang, F., Zhang, H.M., Zhang, J., Zhang, Q., Zhang, T., Zhang, W., Zhang, W.C., Zhang, W.Z., Zhang, Y., Zhang, Y., Zhang, Y.F., Zhang, Y.J., Zhang, Z., Zhang, Z., Zhang, Z.L., Zhao, H.S., Zhao, J.L., Zhao, X.F., Zheng, S.J., Zhu, Y., Zhu, Y.X., Zou, C.L., Insight-HXMT Collaboration: INSIGHT-HXMT Observations of the New Black Hole Candidate MAXI J1535-571: Timing Analysis. *The Astrophysical Journal* **866**(2), 122 (2018) <https://doi.org/10.3847/1538-4357/aade4c> arXiv:1808.05318 [astro-ph.HE]
- [52] Zoghbi, A., Fabian, A.C., Uttley, P., Miniutti, G., Gallo, L.C., Reynolds, C.S., Miller, J.M., Ponti, G.: Broad iron L line and X-ray reverberation in 1H0707-495. *Monthly Notices of the Royal Astronomical Society* **401**(4), 2419–2432 (2010) <https://doi.org/10.1111/j.1365-2966.2009.15816.x> arXiv:0910.0367 [astro-ph.HE]
- [53] Vaughan, S., Edelson, R., Warwick, R.S., Uttley, P.: On characterizing the variability properties of X-ray light curves from active galaxies. *Monthly Notices of the Royal Astronomical Society* **345**(4), 1271–1284 (2003) <https://doi.org/10.1046/j.1365-2966.2003.07042.x> arXiv:astro-ph/0307420 [astro-ph]
- [54] Mizumoto, M., Done, C., Hagino, K., Ebisawa, K., Tsujimoto, M., Odaka, H.: X-ray short-time lags in the Fe-K energy band produced by scattering clouds in active galactic nuclei. *Monthly Notices of the Royal Astronomical Society* **478**(1), 971–982 (2018) <https://doi.org/10.1093/mnras/sty1114> arXiv:1805.00046 [astro-ph.HE]
- [55] Svoboda, J., Dovčiak, M., Goosmann, R.W., Jethwa, P., Karas, V., Miniutti, G., Guainazzi, M.: Origin of the X-ray disc-reflection steep radial emissivity. *Astronomy and Astrophysics* **545**, 106 (2012) <https://doi.org/10.1051/0004-6361/201219701> arXiv:1208.0360 [astro-ph.HE]
- [56] Ingram, A., Mastroserio, G., Dauser, T., Hovenkamp, P., van der Klis, M., García, J.A.: A public relativistic transfer function model for X-ray reverberation mapping of accreting black holes. *Monthly Notices of the Royal Astronomical Society* **488**(1), 324–347 (2019) <https://doi.org/10.1093/mnras/stz1720> arXiv:1906.08310 [astro-ph.HE]

- [57] Shreeram, S., Ingram, A.: Exploring the radial disc ionization profile of the black hole X-ray binary GRS 1915+105. *Monthly Notices of the Royal Astronomical Society* **492**(1), 405–412 (2020) <https://doi.org/10.1093/mnras/stz3455> arXiv:1912.06833 [astro-ph.HE]
- [58] Mastroserio, G., Ingram, A., Wang, J., García, J.A., van der Klis, M., Cavecchi, Y., Connors, R., Dauser, T., Harrison, F., Kara, E., König, O., Lucchini, M.: Modelling correlated variability in accreting black holes: the effect of high density and variable ionization on reverberation lags. *Monthly Notices of the Royal Astronomical Society* **507**(1), 55–73 (2021) <https://doi.org/10.1093/mnras/stab2056> arXiv:2107.06893 [astro-ph.HE]
- [59] Zdziarski, A.A., Johnson, W.N., Magdziarz, P.: Broad-band γ -ray and X-ray spectra of NGC 4151 and their implications for physical processes and geometry. *Monthly Notices of the Royal Astronomical Society* **283**(1), 193–206 (1996) <https://doi.org/10.1093/mnras/283.1.193> arXiv:astro-ph/9607015 [astro-ph]
- [60] Mastroserio, G., Ingram, A., van der Klis, M.: Multi-time-scale X-ray reverberation mapping of accreting black holes. *Monthly Notices of the Royal Astronomical Society* **475**(3), 4027–4042 (2018) <https://doi.org/10.1093/mnras/sty075> arXiv:1801.03100 [astro-ph.HE]
- [61] Lyubarskii, Y.E.: Flicker noise in accretion discs. *Monthly Notices of the Royal Astronomical Society* **292**(3), 679–685 (1997) <https://doi.org/10.1093/mnras/292.3.679>
- [62] Churazov, E., Gilfanov, M., Revnivtsev, M.: Soft state of Cygnus X-1: stable disc and unstable corona. *Monthly Notices of the Royal Astronomical Society* **321**(4), 759–766 (2001) <https://doi.org/10.1046/j.1365-8711.2001.04056.x> arXiv:astro-ph/0006227 [astro-ph]